Simulation of urban temperatures from very high resolution satellite imagery

Thomas Krauß

Remote Sensing Institute DLR, German Aerospace Center 82234 Oberpfaffenhofen, Germany ORCID: 0000-0001-6004-1435

Erwin Lindermeir

Remote Sensing Institute DLR, German Aerospace Center 82234 Oberpfaffenhofen, Germany ORCID: 0000-0003-0929-4378

Abstract—In this work we present a new approach for simulating and estimating temperatures in urban environments solely from very high resolution satellite stereo imagery. For this first a dense digital surface model (DSM) is calculated from two or more satellite stereo images together with a digital terrain model (DTM). The difference gives high objects like buildings and trees. Using also the spectral information from the satellite imagery allows for classification of the scene to different surface materials. The main classes derived for a urban scene contain water, tree, grass, soil, road, adobe tiles and concrete. For each of the classes physical constants like the heat-capacity c in [kJ/kg/K], the heattransport λ in [W/m/K], the density of the material ρ in [kg/dm³], the absorption α (in %) and the diffusion resistance r_l in [s/m] are derived and used for the further simulation. Also for preparing the simulation the sky-view of each pixel in the resulting DSM is calculated together with shadows every 300 seconds for a whole day. Afterwards the simulation runs several times for the day until stability is reached. The results are temperature maps for every 5 minutes for a whole day of 24 hours. Finally the results are compared with independent temperature measurements.

Index Terms—Temperature simulation, Urban heat island, Very high resolution satellite imagery, Dense digital elevation models, Classification of materials

I. Introduction

In the course of climate change extreme weather events get more and more frequent. These do not only include on the one hand more heavy strong rain events but also on the other hand longer and heavier draughts [1]. Especially in urban areas arouse so called "Urban heat islands" (UHI) more often. These urban heat islands are characterized by a much higher temperature in the urban surrounding than in rural regions around cities. These higher temperatures lead also frequently to a huge increase of health risks even until fatal heat strokes especially for elderly people. The topic of Urban Heat Islands is raising rapidly in the last years as can be seen in the papers and topics of the last years "Joint Urban Remote Sensing Events" (JURSE) or even the specially dedicated to this topic "International Conference on Countermeasures to Urban Heat Islands".

So an easy estimation and simulation of expected heat conditions in urban areas is a relevant task for each city administration. In this work we show how a simulation can be performed simply from a set of very high resolution satellite stereo images.

II. EXISTING WORKS

Often used methods for simulation of urban temperatues include computational fluid dynamics (CFD) or the Weather Research and Forecasting model (WRF). Computational fluid dynamics is mostly the base of all urban simulations involving especially wind flow [2]. But the complex urban model design and the long computation times make the use of such models very tedious. On the other hand the WRF model is designed for the use of large scale areas and not for fine urban structure analysis [3]. Actually PALM [4] is the most commonly used tool for simulation of urban atmospheric boundary layers developed as a turbulence-resolving large-eddy simulation (LES) model based also on the Reynolds-averaged Navier-Stokes (RANS) equations. So it's actually the state-of-the-art simulation but it needs also - as every CFD model - a very complex modeling and setup. So we decided to start from scratch and implement a new, simplified model which is based only on one satellite image and a digital surface model (DSM) or a pair of satellite images. All needed parameters for an admittedly much simpler but never the less sufficient urban heat simulation are automatically derived in our proposed approach from the single satellite input data. Since we want to estimate a "worst case scenario" we ignore in our simulation the effects of wind and such the need for complex in-detail CFD simulations.

III. METHOD

From the satellite stereo imagery first a digital surface model (DSM) is derived. This surface model allows the calculation of the shadows for each time on any day in the year. Also we are able to derive a so called sky-view-index from the surface model. This value gives us the percentage of sky which is visible from each point in the DSM. Together from the shadow and the skyview we are able to get the areas and intensities of direct and indirect illumination.

Second from the multispectral satellite images we can derive a coarse classification of materials. For each of these material-classes we can define typical values of physical properties like absorption, reflection, heat conduction or heat capacity. For wet materials like water, grass, soil or – especially – trees we can also estimate a typical diffusion resistance parameter

which allows us to include also evapotranspiration effects in our model.

Based on the DSM, derived shadows and skyview we can simulate the sun illumination – optionally moderated by weather conditions like clouds – for a given day. Based on the sun illumination we calculate the incoming radiation (direct and indirect sunlight) and the outgoing (thermal) radiation. Using also the derived material-classes we are able to simluate heat-convection, heat-conduction and – if it's not a dry surface – also the evaporation of the surface.

A. Preprocessing of the satellite data

The first step of the proposed processing chain is the derivation of a dense digital surface model (DSM) using the semi-global-matching algorithm as shown in [5] from at least two very high resolution stereo images. Afterwards a digital terrain model (DTM) representing only the ground without elevated objects like buildings or trees is calculated from the DSM. Using the DSM, the DTM and the orthorectified, pan-sharpened multispectral satellite image allows a coarse classification of the satellite data. Fig. 1 shows the test area in Hamburg. On the left the ortho image derived from the original WorldView-4 satellite image is displayed. In the center the derived DSM and on the right the classification.







Fig. 1. Test region Hamburg, $3 \times 3 \text{ km}^2$, left: Ortho image from the WorldView-4-scene, center: derived DSM, right: derived classification (blue: water, light-green: grass, dark-green: tree, red: adobe roof tiles, light-gray: concrete on flat roofs, dark-grey: asphalt/road, yellow: bare soil).

For the classification a normalized difference vegetation index (NDVI) is calculated from the red and the near-infrared band as NDVI = (nir - red)/(nir + red). The NDVI is above a certain threshold (e.g. 0.2) for vivid vegetation and below an other threshold (e.g. -0.1) for water. Using also the object height as difference of the DSM and DTM and other spectral properties like hue and saturation together with slopes from the DSM and the object heights gives the following classes:

- water: NDVI low (blue)
- grass: NDVI high, height low (light green)
- tree: NDVI high, height high (dark green)
- adobe: red, height high, slope not flat (red)
- concrete: gray, height high, slope flat (light gray)
- road: gray, height low, slope flat (dark gray)
- soil: soil-spectrum, height low (yellow)

For each of these classes typical material parameters are estimated and stored in the materials map ${\cal M}_{x,y}$ consisting of the five bands

- c heat-capacity in [kJ/kg/K],
- λ heat-transport in [W/m/K],
- ϱ density of the material [kg/dm³],
- α absorption of the surface material (unitless, from 0...1),
- r_l diffusion resistance in [s/m].

If r_l is set to 0 it is a dry material and no evaporation term is taken into account. A value of 1 denotes an open water surface while values of 200 to 2000 can be used for leaves of trees or grass.

Beneath this material map also following inputs of the same size as the DSM $D_{x,y}$ and the material map $M_{x,y}$ are generated for the simulation:

 $S_{x,y,t}$ shadow mask, 0=shadow, 1=illuminated, calculated every 5 min. for the whole simulated day

 $V_{x,y}$ sky-view from 0...1 (for indirect illumination)

 $\vec{V}_{x,y}$ surface normal for each pixel derived from $D_{x,y}$ (needed for the calculation of lambertian illumination)







Fig. 2. Same test region Hamburg, 3×3 km², left: shadow 2018-10-05 at 10:30 UTC, center: mean of all shadows of the day, right: skyview.

Fig. 2 shows the derived shadow $S_{x,y,1030}$ for 10:30 UTC of the acquisition date of the WorldView image (2018-10-05), a mean of all shadows of the day and also the derived skyview $V_{x,y}$. The skyview contains values of 100 % for points from which the whole sky hemisphere is visible (white) down to 0 % for areas from which no sky can be seen (black).

B. Simulation of temperatures

For the simulation a multi-layer temperature profile image of the same size as the inputs $D_{x,y},\,M_{x,y},\,\dots$ is created as shown in fig. 3. It consists of a surface layer and e.g. five substrate-layers of a depth of $d_s=5$ cm each below the surface and also five air-layers of $d_a=50$ cm each above the surface. The surface and substrate layers have for each pixel (x,y) the unique material constants from the material map. All air-layers are modeled with the same physical constants for "air" independent of the position in the image.

Beneath the material-constants for each pixel of the image also some global scene constants are needed:

- A area of one pixel [m²], known from the resolution of the imagery
- $\vec{d}_{S,t}$ sun direction as vector automatically derived from sun-azimuth $a_{S,t}$ and -zenith $z_{S,t}$ angles, changing in time t during simulation
- ε emissivity of surface to longwave radiation (0.91)

k Stefan-Boltzmann constant $5.67 \cdot 10^{-8}$ [W/m²K⁴] C_S solar constant of 1000 [W/m²]

 T_{back} thermal back-scattering of atmosphere (0.7, unitless)

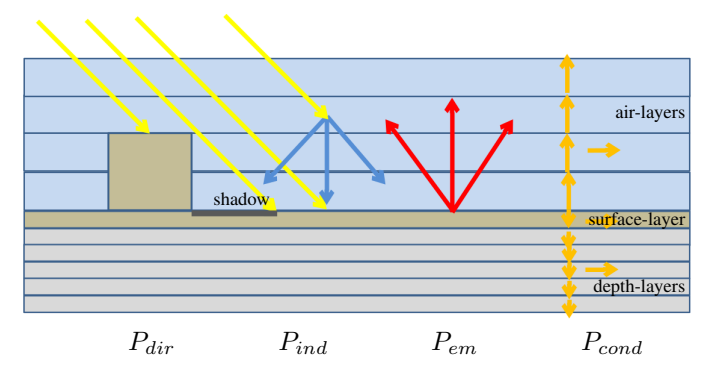


Fig. 3. Illustration of the model used with one surface-layer and two sets of air- and depth-layers of different depths.

Fig. 3 illustrates the model used. The simulated heat flow per time $Q/\Delta t = \Delta P$ consists of

 P_{dir} the direct incoming radiation in non-shadow areas, P_{ind} the indirect radiation also in shaded areas depending on the skyview-factor,

 P_{em} the thermal emission and also the loss of heat due to evaporation,

 P_{cond} the heat-conduction in the material and heat-convection in the air-layers.

The simulation is based on an iterative calculation of a new temperature $T_{i,l,x,y}$ for each pixel (x,y) and each of the temperature layers l in iteration i. The new temperature $T_{i+1,0,x,y}$ on the surface is calculated from the previous T_i and the differences of incoming and outgoing heat-flows ΔP in Watt [W] for a time-step Δt as:

$$T_{i+1} = T_i \cdot \Delta P \cdot \frac{\Delta t}{c \cdot m} \tag{1}$$

with the heat-capacity $c_{x,y}$ of surface pixel (x,y) in [kJ/kg/K] and the mass of this surface-pixel as $m=\varrho_{x,y}\cdot A\cdot d_s$. The components which contribute to ΔP are

$$P_{dir} = I_L C_S A \alpha S \tag{2}$$

$$P_{ind} = I_a C_S A \alpha \tag{3}$$

$$P_{em} = \varepsilon k T_i^4 A + L(T_i) E A \tag{4}$$

$$P_{cond,l<1} = \lambda_{x,y} A(T_{i,l,x,y} - T_{i,l-1,x,y}) / d_s$$
 (5)

$$P_{cond,l=1} = \lambda_{air} A(T_{i,0,x,y} - T_{i,1,x,y}) / d_a$$
 (6)

$$+k_1\sqrt{\frac{v}{D}}(T_{i,0,x,y}-T_{i,1,x,y})$$
 (7)

$$P_{cond,l>1} = \lambda_{air} A(T_{i,l,x,y} - T_{i,l+1,x,y})/d_a$$
 (8)

(9)

with shadow mask $S_{x,y}$, lambertian illumination $I_L = \vec{d}_S \cdot \vec{N}_{x,y}$ and ambient illumination $I_a = (0.2V_{x,y} + 0.8)\frac{2}{3}\cos z_S$. L(T) is the latent heat of vaporization of water in [J/kg]

(around $2.5 \cdot 10^6$ J/kg, slightly depending on the temperature) and E the transpiration rate of wet surfaces in [kg/m²s] given as function of the surface temperature T_s , the temperature of the lowest air-layer T_a and the relative humidity rh as

$$E(T_s, T_a, rh) = \frac{\varrho_v(T_s, rh) - rh \cdot \varrho_v(T_a, rh)}{r_l + k_2 \sqrt{D/v}}$$
(10)

with ϱ_v the vapor density of saturated air in [kg/m³] depending on the temperatur T_a and the relative humidity rh, r_l as the diffusion resistance in [s/m] given in the material-map, a leaf-diameter D, a wind-speed v and a experimentally derived constant $k_2 = 200\sqrt{\rm s/m}$. Due to missing detailled information on leaf-sizes and local wind-speeds the factor D/v is set without loss of generality to 1.0. All details can be changed by setting r_l in the material map properly. If r_l is set to 0 this is interpreted as "dry surface" and E is set to zero. Also E is set to zero for surfaces with temperatures below 0° C (water is frozen).

The parameters for $P_{cond,l}$ for each layer l (l=0 is the surface, l<0 is depth and l>0 is air) are the heat-transport $\lambda_{x,y}$ from the material-map for surface and depth and λ_{air} constant for all air-layers. d_s is again the depth of a "depth"-layer while d_a is the height of all air-layers. On the surface additionally a loss of convection proportional to a constant $k_1=9.14\mathrm{W}\sqrt{\mathrm{s}/\mathrm{K}}$ and the default v/D=1.0 are used.

Also in air-layers two kinds of absorption from the emission of surface P_s and from absorption of sun-radiation P_r occurs. On the other hand also emission P_e occurs for each air-layer following

$$P_s = \frac{4}{3}\varepsilon\alpha_s \cdot A \cdot k \cdot (T_s^4 - T_{air}^4) \cdot \alpha_{air}$$
 (11)

$$P_r = I_L C_S A \alpha_{air} S \tag{12}$$

$$P_e = \varepsilon k T_{air}^4 A \tag{13}$$

$$\Delta T_{air} = (P_s + P_r - P_e) \frac{\Delta t}{c_{air} \cdot m_{air}}$$
 (14)

Here I_L is not really correct to use for P_r , but it's used for simplicity since it includes also night- (then it's 0), direct- and indirect-radiation-factors.

IV. RESULTS AND DISCUSSION

Figure 4 shows the results of the simulation for a small section of $240 \times 150~\text{m}^2$ from the above mentioned test area Hamburg. The satellite image was a pan-sharpened WorldView-4 image with a ground resolution of 30 cm, acquired at 2018-10-05 at 10:38 UTC. The figure shows the simulated temperatures for this area at four times: at 00:00, 06:00, 12:00 and 18:00 UTC. For this day the sun rises in Hamburg at 05:40 UTC (first shadow) and sets at 16:35 (last shadow).

For comparison with the simulation results we use the actual weather conditions from open-meteo.com for the simulated date 2024-10-05 including cloud cover, the soil (or surface) temperature and a temperature 2 m above ground, which corresponds to our fourth air-layer.

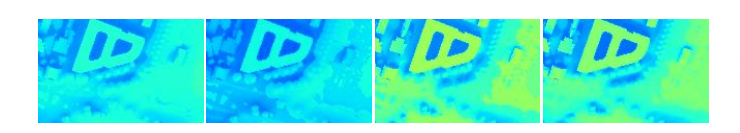


Fig. 4. Simulation results for a section $240\times150~\text{m}^2$ from the Hamburg scene for 2024-10-05 at 00:00, 06:00, 12:00 and 18:00

Figure 5 show the temperature profiles over the layers for four specified points. Shown are the layers on the vertical axis. The surface layer is at 0, the depth layers are -1 to -5 with a depth of 5 cm each, the air-layers are from 1 to 5 with a height of 50 cm each. On the horizontal axis the temperatures are displayed. The temperature profiles are shown at two hours steps denoted for each profile above (am) or below (pm) the temperature at the surface layer.

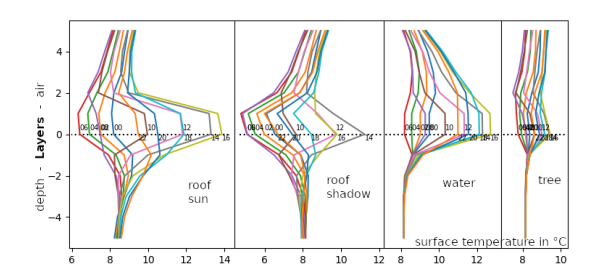


Fig. 5. Simulated temperature profiles for sunlit roof, shadowed roof, water and tree surface

Shown are the temperature profiles for points at an adobe roof, for water and a tree. The first plot shows a mostly sunlit roof in southward direction, the second a point on the northern side of the roof, the third the profiles over a water surface and the fourth on a tree. As can be seen the roof towards the south heats up much quicker and longer than the north facing roof. Comparing the behaviour of the depth-/material-layers of the adobe roof-tiles and the water shows also clearly the much lower heat conduction and higher heat capacity of the water in contrast to the roofs. Already in the first layer below the surface the temperature in the water varies over the day only 0.6 K from 8.6 to 9.2°C while the range in the tiles varies over 2.3 K from 6.5 to 8.8°C. The tree shows only a small variation of temperatures between 7.8 and 9.4°C on the surface and also a very low variation at the first depth layer of only 0.5 K.

V. CONCLUSION AND OUTLOOK

In the presented work we described a simplified approach for simulating temperatures over an urban area solely using one or more very high resolution satellite images as inputs. From the satellite data a digital surface model (DSM) and also a simplified material classification is derived. Using the DSM the shadows for every five minutes of a day can be calculated. Also slopes and the skyview are derived. The material classification is based on the multispectral pan-sharpened satellite image together with the slopes and the heights above ground. For each classified material typical physical values like density, absorption, heat conduction and heat capacity are stored in the materials-map.

In a second step the simulation runs on these derived phyical material data building up a surface layer and a number of substrate- and air-layers. For each of the layers the temperature is iterated calculating incoming and outgoing radiation, heat flows, heat conduction and convection. Also the transpiration of wet surfaces – especially the leaves of trees – is included in the simulation.

The first results of the simulation show reasonable values and behaviour of the different modeled materials. The results compare well to measured temperatures over the test area. But for a better refinement and calibration of the model it has to be evaluated with fine-grained in-situ temperature measurements of different cities in different climates. For a better modelling also a layer for relative humidity should be included.

REFERENCES

- [1] J. Tollefson, "IPCC climate report: Earth is warmer than it's been in 125,000 years," *Nature*, vol. 2021, no. 596, pp. 171–172, 2021.
- [2] S. Du, X. Zhang, X. Jin, X. Zhou, and X. Shi, "A review of multi-scale modelling, assessment, and improvement methods of the urban thermal and wind environment," *Building and Environment*, vol. 2013, p. 108860, 2022
- [3] H.-C. Zhu, C. Ren, J. Wang, Z. Feng, F. Haghighat, and S.-J. Cao, "Fast prediction of spatial temperature distributions in urban areas with WRF and temporal fusion transformers," *Sustainable Cities and Society*, vol. 103, p. 105249, 2024.
- [4] B. Maronga, M. Gryschka, R. Heinze, F. Hoffmann, F. Kanani-Sühring, M. Keck, K. Ketelsen, M. O. Letzel, M. Sühring, and S. Raasch, "The Parallelized Large-Eddy Simulation Model (PALM) version 4.0 for atmospheric and oceanic flows: model formulation, recent developments, and future perspectives," *Geosci. Model Dev.*, vol. 8, pp. 1539–1637, 2015. [Online]. Available: https://palm.muk.uni-hannover.de/
- [5] P. dAngelo and P. Reinartz, "Semiglobal Matching Results on the ISPRS Stereo Matching Benchmark," in *International Archives of Photogram-metry and Remote Sensing*, vol. XXXVIII-4/W19, 6 2011, pp. 79–84.